

HYBRID RANS-LES MODELLING OF TURBULENT FLOW AROUND A
THREE-ELEMENT AIRFOIL

Shia-Hui Peng*

Department of Computational Physics,
Swedish Defence Research Agency, FOI
SE-164 90 Stockholm, Sweden
peng@foi.se

ABSTRACT

An algebraic hybrid RANS-LES (HYB0) model was applied to the A310 high-lift three-element configuration at a freestream Mach number of $M_\infty = 0.22$. Computations were conducted for two different angles of attack at $\alpha = 12.2^\circ$ and $\alpha = 25.2^\circ$, respectively, with or without prescribed transition around the leading edges of the slat, main wing and flap. At $\alpha = 25.2^\circ$, wind tunnel test indicated a stalled flow with a sudden drop in lift. The computations were compared with measured pressure distributions and, at the stall angle, with the S-A DES computation as well. It was shown that the modelling may significantly be affected by the transition specified around the leading edges, for which the eddy viscosity was switched off in the laminar boundary layer. With prescribed transition, the S-A DES model pronounced undesired boundary layer separation on the slat upper surface. For full-turbulence computations, the modelling tends to pronounce a delayed stall at a relatively large incidence. Provided that the uncertainties could be ruled out at large incidences, the modelling performance should be justifiable to scrutinize the properties of high-lift flows towards and at stall. At $\alpha = 12.2^\circ$, where the location of transition was experimentally affirmed, it was shown that hybrid modelling was able to produce reasonable predictions with appropriate grid resolution.

INTRODUCTION

In order to accurately represent the complex flow properties around high-lift devices in aerodynamic applications, turbulence modelling remains a challenging issue. This is particularly true for flows around multi-element wings of different type at large angles of attack, where the turbulent flow is often characterized by boundary layer transition, confluence of boundary layers, as well as by boundary layer separation and trailing wakes. Giving further complications at large incidences approaching stall and beyond, the flow around a multi-element wing becomes unsteady with massive vortex motions.

Conventional RANS approaches have been widely employed for high-lift flows, ranging from linear eddy viscosity formulation to Reynolds stress models. While different degrees of success have been reported, some noticeable shortcomings and uncertainties have also been highlighted by Rumsey et al. (Rumsey and Gatski, 2001; Rumsey and Ying, 2002). Many of previous simulations, moreover, invoked steady RANS modelling even at large angles of attack beyond the maximum lift, implying additional uncertainties in analysis of inherently unsteady flow properties. Being potentially capable of resolving high-lift flows (in particular, at

large incidences), on the other hand, large eddy simulation (LES) may become very (if not prohibitively) costly at relatively high Reynolds numbers. It is well known that the grid resolution is considerably demanding to reach reliable LES modelling. This has been well demonstrated in a previous EU project LESFOIL (Davidson et al., 2003) for the flow around a single airfoil at a moderate Reynolds number.

The presence of the detached eddy simulation (DES) by Spalart et al. (1997) and the subsequent development of other hybrid RANS-LES modelling methods have made it possible to investigate the flow properties around a multi-element wing configuration at high Reynolds numbers relevant to aerodynamic applications, by means of cost-effective computations. This is particularly justifiable and feasible to resolve unsteady vortex motions stemmed from boundary layer separation on the configuration surface. Recently, several computations of high-lift flows have been reported using the S-A DES or similar approaches see, e.g., Cummings et al. (2004) and Deck (2005). We have lately performed a number of URANS computations for the A310 three-element airfoil at stall (Peng and Eliasson, 2008), where a preliminary presentation of DES modelling was also given for comparison. It was shown that URANS modelling pronounced periodically unsteady flows being stalled instantly, at which the instantaneous lift matches well with the experimentally measured stall lift. Sensible discrepancies were observed, however, in the predicted time-averaged mean flow, which may significantly be affected by the transition prescribed around the leading edges of the elements, with the DES modelling (Peng and Eliasson, 2008).

One of the main purposes with the present work is to examine the modelling performance of an alternative hybrid RANS-LES method for the flow around the same A310 three-element configuration. The computation explores further the resolved flow properties and investigates the modelling feasibility in terms of the effect of prescribed local transition and different modelling approaches. Two different angles of attack have been considered in the computations with, respectively, massive and moderate boundary layer separations on the upper surface of the three-element airfoil. In the following sections, the simulation methods are first presented, which is followed by a presentation of results, and subsequently, some conclusions are given.

SIMULATION METHODS

The algebraic hybrid model (hereafter **HYB0 model**), used in the present work, employs a simple mixing-length-type RANS model near the wall in combination with the Smagorinsky SGS model away from the wall, by means of an adaptation of turbulent length scales derived from the RANS and LES modes. The model has been extensively

*Also Department of Applied Mechanics, Chalmers University of Technology, Sweden

calibrated and validated in previous work, see e.g. Peng (2005, 2006) and Peng and Leicher (2008). Only is a brief description presented below for the modelling formulation.

The turbulent stress tensor is identically denoted here with τ_{ij} , resulting from either time averaging or spatial filtering to the Navier-Stokes equations, which is formulated in the form of

$$\tau_{ij} = -2\mu_h \left(S_{ij} - \frac{1}{3}\delta_{ij}S_{kk} \right) + \frac{1}{3}\delta_{ij}\tau_{kk} \quad (1)$$

where μ_h is the *hybrid* eddy viscosity for the hybrid model and S_{ij} is the strain rate tensor, $S_{ij} = (\partial u_i/\partial x_j + \partial u_j/\partial x_i)/2$. For modelling compressible flows, the transport equation for the total energy, E , is solved, in which a model for the turbulent heat flux vector is incorporated. In the present computation, we have adopted the eddy diffusivity model for both the RANS and LES modes, namely,

$$h_k = -\frac{\mu_h}{Pr_h} \frac{\partial T}{\partial x_k} \quad (2)$$

where Pr_h is the turbulent Prandtl number. A value of $Pr_h = 0.4$ has been used in both the LES and the RANS regions.

For the near-wall RANS mode, the mixing-length concept is used to formulate the eddy viscosity by

$$\tilde{\mu}_t = \rho \tilde{l}_\mu^2 |S| \quad (3)$$

where the length scale, \tilde{l}_μ , is proportional to the wall distance d , reading $\tilde{l}_\mu = f_\mu \kappa d$ and $\kappa = 0.418$ being the von Kármán constant. To avoid the awkwardness of using wall-shear related parameters in the formulation when modelling separating and/or reattaching flows, the empirical damping function f_μ is formulated in terms of the RANS turbulent Reynolds number, $R_t = \tilde{\mu}_t/\mu$, viz.

$$f_\mu = \tanh \left(\frac{R_t^{1/3}}{2.5} \right) \quad (4)$$

In the off-wall LES region, the SGS eddy viscosity with the Smagorinsky model reads

$$\mu_{sgs} = \rho (C_s \Delta)^2 |S| \quad (5)$$

with $C_s = 0.12$ and $\Delta = \sqrt{(\Delta_{max}^2 + \delta V^{2/3})/2}$, where δV is the control volume of a local node and Δ_{max} is the local maximum cell size, $\Delta_{max} = \max(\Delta_x, \Delta_y, \Delta_z)$. Note that, with a uniform structured grid, $\Delta = \delta V^{1/3}$, which is the conventional filter width used in LES. With unstructured meshes, Δ_{max} has been estimated by taking the largest edge size of each node. For convenience, note that the over-bar above a flow variable has been dropped, which has otherwise been conventionally used to denote a spatial-filtered flow quantity in LES.

The matching between the RANS and LES modes is accomplished by adapting the RANS turbulent length scale over the RANS-LES interface into $l_\mu = \tilde{l}_\mu f_s$ so that $\mu_t = \rho l_\mu^2 |S|$ in the RANS region, where f_s is an empirical matching function and reads

$$f_s = \frac{1}{2} \left[\exp \left(-\frac{R_s^{0.75}}{4.75} \right) + \exp \left(-\frac{R_s^{0.3}}{2.5} \right) \right] \quad (6)$$

In Eq. (6), $R_s = \tilde{\mu}_t/\mu_{sgs}$, which is the ratio between the intensities of RANS-modelled turbulence and SGS-modelled turbulence. The use of the function, f_s , is to achieve a

smooth transition for the RANS-LES length-scale adaptation, which makes the near-wall RANS mode produce interfacing turbulence that is comparable to the *resolved-turbulence* in order to attain a realistic matching with the off-wall LES mode.

The eddy viscosity, μ_h , in the HYB0 model is computed by

$$\mu_h = \begin{cases} \mu_t & \text{if } \tilde{l}_\mu < \Delta \\ \mu_{sgs} & \text{if } \tilde{l}_\mu \geq \Delta \end{cases} \quad (7)$$

A problem encountered with other DES approaches is the so-called "modelled-stress depletion" (MDS), which may be caused by local grid refinement in such a way (inappropriately) that the LES-mode penetrates into the boundary layer and triggering a reduced eddy viscosity and modelled stresses. This has been regarded as being the major cause of the unphysical "grid-induced separation" (GIS). It is noted here that the use of f_s in the HYB0 model may to some extent help to remedy the problem as such. Provided that the LES-region is *pushed* toward the near-wall region for grid refinement, the SGS eddy viscosity would be reduced accordingly, as shown in Eq (5). This will consequently induce small values of f_s , and subsequently rendering reduced μ_t for the RANS mode. As a consequence, the turbulence content triggered by the RANS mode is sustained and comparable to the LES-resolved turbulence over the RANS-LES interface. In the limit of subsequent grid refinement, on the one hand, Eq. (7) suggests that the LES region shrinks onto the wall surface; on the other hand, f_s (and thus μ_t) approaches zero, giving overall LES modelling with the Smagorinsky model.

The HYB0 model is incorporated into a compressible CFD code, which is a node-based unstructured Navier-Stokes solver for the compressible flow equation system using finite volume method. Both the convective and viscous fluxes are approximated with the second-order central scheme. A dual time-stepping method is employed, in which the physical time is advanced using a second-order implicit scheme, while at each time step the governing equations are integrated toward convergence with a 3-stage Runge-Kutta scheme using local time steps and implicit residual smoothing. The convergence is accelerated with agglomeration multigrid method, for which an injection operator is used for prolongation, and its transpose for restriction.

The landing configuration of the unswept three-element airfoil is studied, which is exposed to a freestream flow of $M_\infty = 0.22$ with a chord-based Reynolds number of $Re = 4.1 \times 10^6$. Experimentally measured pressure distributions are available for several different angles of attack (AoA). At small incidences, laminar-turbulence transition was observed around the leading edges of the elements composed in the configuration. This is however not affirmed at large AoA, for example, at the experimentally observed stall angle. In the computations with either the HYB0 or the S-A DES model, the laminar boundary layer has been prescribed by setting the modelled eddy viscosity to zero.

Two angles of attack have been considered in the computation, namely, $\alpha = 12.2^\circ$ and $\alpha = 25.2^\circ$, respectively, of which the latter is the stall angle according to the experimental observation.

A 2D grid was first generated with a refined mesh around the configuration surface and in regions where anticipated trailing wakes may arise. The 3D grid was then generated by distributing the 2D grid in the spanwise direction with uniform spacings. In some preliminary computations, the effect of spanwise extension, Z_{max} , was investigated by taking

$Z_{max} = 0.2C$ and $Z_{max} = 0.4C$, respectively, where C is the chord of the retracted configuration. With the same grid resolution in the spanwise direction, the effect of Z_{max} was insignificant using either of the two sizes. The results presented in this work have been obtained using $Z_{max} = 0.2C$. In addition, the effect of grid refinement in the spanwise direction was explored for $\alpha = 12.2^\circ$, using 24 and 48 cells in this direction, which gave about 2 and 4 million nodes in total for the 3D grid, respectively. The configuration is placed in the center of a $100C \times 100C$ domain. The characteristic boundary condition was used for the far-field boundary and periodic conditions were assumed in the spanwise direction.

In Figure 1, a schematic of the computational grid around the three-element airfoil is illustrated. Note that a layer of prismatic cells has been clustered in the wall layer.

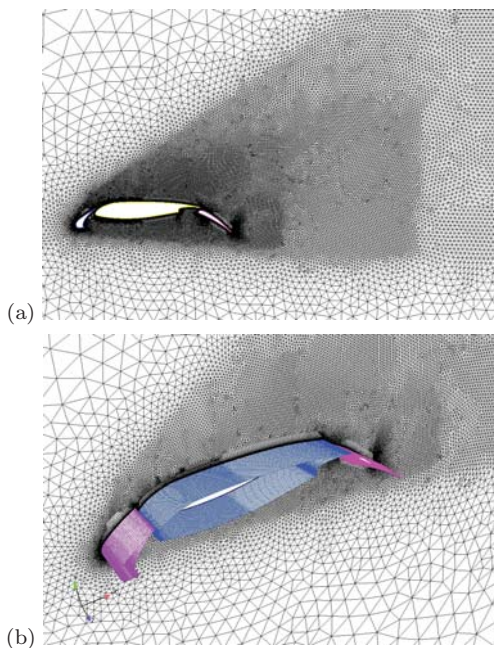


Figure 1: Schematic of the computational grid around the three-element airfoil. (a) Grid in a 2D section; (b) Overview of the 3D grid with uniform spacings in the spanwise direction.

The computation started with an initial field obtained from either a RANS computation or a previous DES computation. After a sufficiently long time period until the resolved flow was fully developed, the statistical analysis was then started to obtain time-averaged solutions. A typical time period for statistic averaging takes about 6-10 convective time of a fluid particle over the high-lift device computed.

RESULTS AND DISCUSSION

With a preliminary presentation of the DES results at $\alpha = 25.2^\circ$, Peng and Eliasson (2008) have shown that the DES modelling may become rather sensitive to the specified transition around the leading edges of the three elements. The DES results are further disseminated and explored here-with. Figure 2 illustrates the mean flow streamlines from the DES computation with prescribed transition, which indicates a boundary layer separation on the suction side of the slat and the main wing,

The flow separation illustrated in Figure 2 is undesirable and is not observed in the DES computation with full-turbulence assumption (Peng and Eliasson, 2008) A close exploration is given in Figure 3, which highlights the stream-

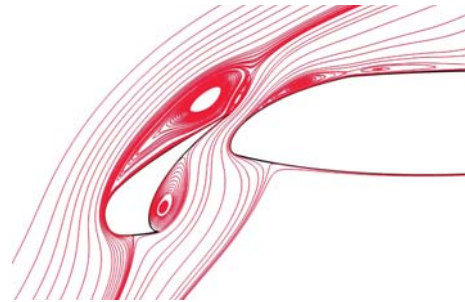


Figure 2: DES computation (transition specified) for $\alpha = 25.2^\circ$. Streamlines for the time-averaged mean flow.

lines colored with $R_t = \mu_t/\mu$, as well as the velocity field and the grid resolution in the boundary layer around the separation point. It is evident that a laminar boundary layer separation is triggered first, which is subsequently exaggerated by a large turbulent separation bubble above the slat surface and accompanied by another boundary layer separation on the main wing surface (see Figure 2)

Note that the cell size in the streamwise direction is generally larger than the boundary-layer thickness, which suggests that the boundary layer has been accommodated by the S-A RANS mode. The flow separation is thus not caused due to inappropriate grid design, namely, it is not a "grid-induced separation" (GIS) as encountered sometimes in S-A DES modelling.

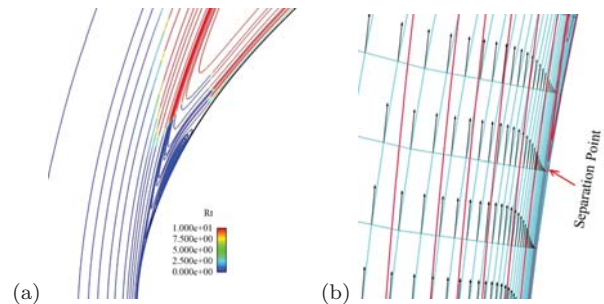


Figure 3: DES computation (transition specified) for $\alpha = 25.2^\circ$. A close view of the time-averaged resolved flow separation over the suction side of the slat. (a) Streamlines colored by $R_t = \mu_{des}/\mu$. (b) Boundary layer and grid resolution around the separation point.

The undesired effect of prescribed transition on the DES modelling has motivated further computations using the HYB0 model with the same grid. Figure 4 illustrates an example of the resolved instantaneous turbulent structure, which has highlighted the unsteady vortex motion after the main wing and in the trailing region.



Figure 4: Illustration of resolved instantaneous vortex motion with the HYB0 model ($\alpha = 25.2^\circ$).

With transition specified at the leading edges of the slat, main wing and flap, respectively, the computation with the

HYB0 model shows different performance, as compared to the DES modelling. The time-averaged mean flow renders no boundary layer separation on the suction side, and the flow is overall attached, as shown in Figure 5. As compared with the DES simulation illustrated in Figure 3, it is obvious that the HYB0 model has responded to the prescribed transition in a different way. Note that, with both models, the transition has been specified by switching off the turbulent eddy viscosity in the same laminar regions around the leading edges. The different responses may be attributed to the history effect in the S-A DES model, which solves for the eddy viscosity from a transport equation, while the HYB0 model is an algebraic model accounting for no history effects of the modelled turbulence. A different method may be needed to specify the laminar boundary layer in the S-A DES modelling.

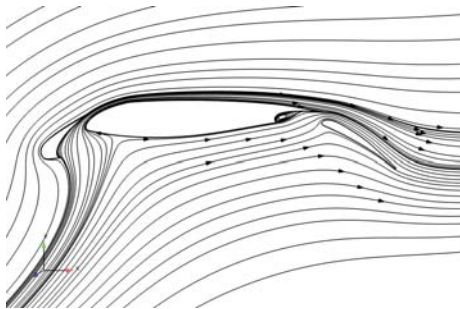


Figure 5: Time-averaged mean streamlines with the HYB0 model (transition specified) for $\alpha = 25.2^\circ$.

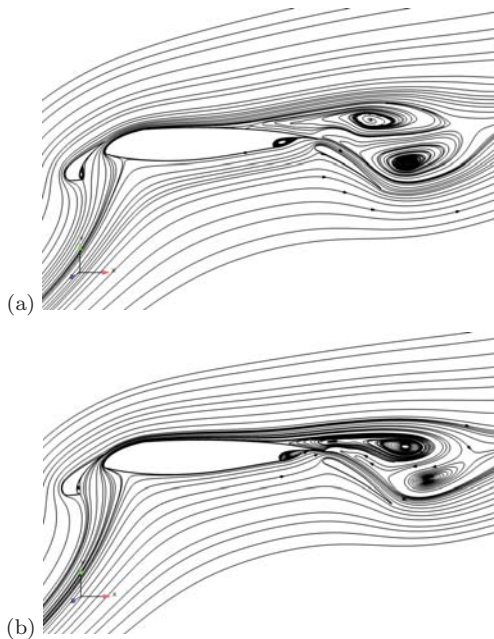


Figure 6: Time-averaged mean streamlines from computations with no transition specified for $\alpha = 25.2^\circ$. (a) HYB0 model. (b) S-A DES model.

In order to further examine the effect of the specified transition on the modelling, full-turbulence computations have been carried out with both the HYB0 and the S-A DES models by turning off the transition specification. The time-averaged mean flow streamline is presented in Figure 6 (a) for the HYB0 model, and in Figure 6 (b) due to the DES model. It is shown that both models have produced similar mean flow properties, significantly different from the

simulations with transition specified, as illustrated in Figure 2 (DES model) and in Figure 5 (HYB0 model). Both the DES and HYB0 models have claimed an attached flow over the upper surface of the slat and of the fore part of the main wing. A pair of separation bubbles are present due to the flow separation stemmed from the rear part of the main wing, which exhibits instantaneous vortex shedding. With a pair of somewhat larger separation bubbles, the boundary layer separation due to the HYB0 model occurs earlier than with the DES model. It is noticed that on the flap upper surface the boundary layer is attached, due to the filled-in flow from the pressure side through the flap gap.

The predicted flow characteristics are reflected in the pressure distribution, as shown in Figure 7, where the measured data at a different incidence, $\alpha = 24.4^\circ$, smaller than the measured stall angle at $\alpha = 25.2^\circ$, are also included for comparison. It is noted here that, because the publication of the experimental details is restricted, only the scale of C_p distributions is given for the y -axis in the respective caption of Figure 7 for $\alpha = 25.2^\circ$ and of Figure 10 for $\alpha = 12.2^\circ$.

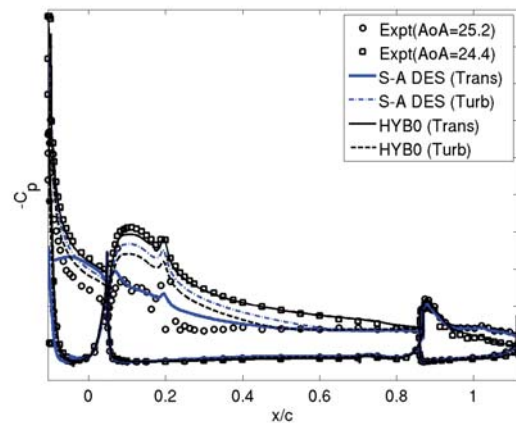


Figure 7: Comparison of pressure distributions at $\alpha = 25.2^\circ$. The scale of C_p on the y -axis is 5.0.

With the DES model and prescribed transition, the undesired flow separation on the slat has made the peak of $-C_p$ eliminated around the slat leading edge. Nonetheless, this computation has rendered a closer agreement with the experimental data at $\alpha = 25.2^\circ$ after the leading edge of the main wing, where a boundary layer separation is disclosed as shown in Figure 2. With prescribed transition, the S-A DES model has produced the earliest flow separation and the largest separation bubble (of all the DES and HYB0 computations) on the upper surface of the main wing (see Peng and Eliasson (2008)), which corresponds well to the pressure distribution shown in Figure 7. The DES computation with full turbulence, on the other hand, has enabled an improved prediction for the slat surface pressure (the peak value of $-C_p$ is still somewhat under-predicted though), whilst lower surface pressures are pronounced on the fore part of the main wing.

In the full-turbulence computation, the HYB0 model has claimed a pressure distribution similar to the DES model, but the predicted surface pressure is somewhat lower than the DES prediction over the upper surface of the slat and the fore part of the main wing. The prediction of surface pressures corresponds well to the flow separation on the wing surface, which occurs at about 55% of the main wing chord from the leading edge for the HYB0 model and about 69% for the DES model (cf. Figure 6). With prescribed tran-

sition, consistent to the predicted mean flow property (cf. Figure 5), the HYB0 model has produced the smallest surface pressures (largest $-C_p$), which falls on the experimental data at $\alpha = 24.4^\circ$ in the overall upper surface of the whole configuration.

As mentioned, there exist some uncertainties in the wind tunnel test at large AoA. The transition location is an observation for smaller incidences but not affirmed at the measured stall angle. Moreover, the measured data may have been affected for 3D motions at large incidences (Rudnik et al., 2005), due to dramatic flow separation and large-scale vortex motions. This is difficult to account for in wind-tunnel corrections for the experimental data. Taking into account these uncertainties, we believe that the modelling with both the HYB0 and the DES model has enabled reasonable performance for the high-lift flow approaching the stall point, except for the DES computation with prescribed transition. In view of the pressure distribution computed at $\alpha = 25.2^\circ$, it is anticipated that the HYB0 model (with or without prescribed transition), as well as the DES model (for full turbulence), would claim a stall at an angle of attack beyond $\alpha = 25.2^\circ$. The HYB0 model with full-turbulence computation may pronounce a stalled flow at an incidence closer to $\alpha = 25.2^\circ$, whilst with prescribed transition this model may conclude a larger stall angle. Further investigation will be conducted with the HYB0 model at AoA larger than $\alpha = 25.2^\circ$ to explore the stalled flow properties around the multi-element configuration.

The uncertainties nestled in the experimental measurement make it somewhat difficult to justify the predictions. Additional computations have thus been conducted for $\alpha = 12.2^\circ$, using the HYB0 model with prescribed transition. At this relatively small incidence, the aforementioned uncertainties in wind tunnel test should have been ruled out. The experimentally observed location of transition is applicable for the computation and the wind-tunnel side-wall effect is expected to be insignificant.

The computational grid is based on the same 2D mesh, as shown in Figure 1, being uniformly distributed in the spanwise direction. In order to highlight possible effects of grid resolution, two different cell spacings have been tested by distributing 25 and 49 nodes in the spanwise direction over a distance of $0.2C$, respectively.

In Figure 8, an example of the resolved instantaneous vortex motion is illustrated to highlight the trailing wake motion after the flap. The iso-surface of vorticity is colored by the modelled turbulence Reynolds number in terms of $R_t = \mu_t/\mu$. Moderate instantaneous vortex shedding is observed. The turbulent structure is elongated in the streamwise direction with less coherence in the spanwise direction.



Figure 8: Resolved instantaneous vortex motion with the HYB0 model (with prescribed transition) at $\alpha = 12.2^\circ$.

Figure 9 displays the streamlines from the time-averaged mean flow. Unlike in the prediction at $\alpha = 25.2^\circ$, where the boundary layer separation occurs on the main wing surface, at $\alpha = 12.2^\circ$ the HYB0 model has pronounced a boundary

layer separation on the flap upper surface near the trailing edge. Both the fine and the coarse grids have produced very similar flow properties, as illustrated in Figure 9 (a) and (b), but that the flow recirculation bubble in the slat cave is more pronounced with the fine grid.

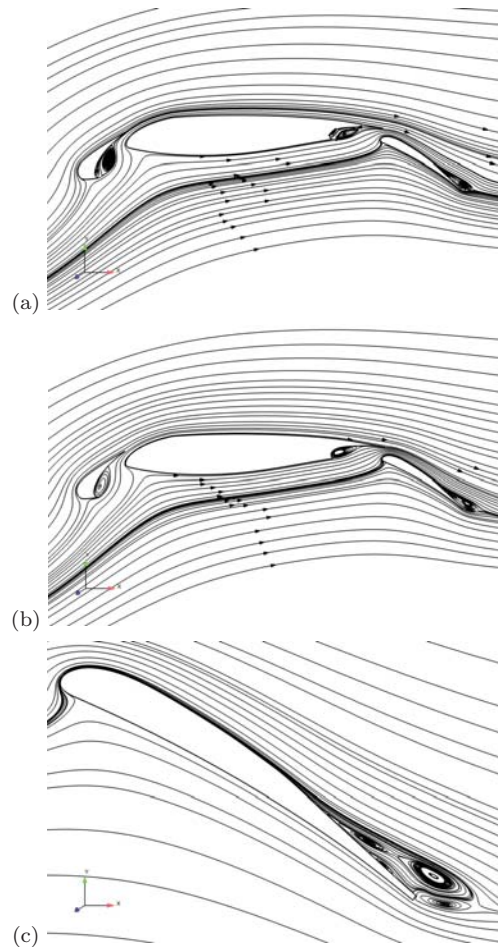


Figure 9: Time-averaged flow streamlines computed with the HYB0 model (with prescribed transition) for $\alpha = 12.2^\circ$. (a) With the fine grid; (b) With the coarse grid; (c) A close view of the flow separation on the flap trailing edge.

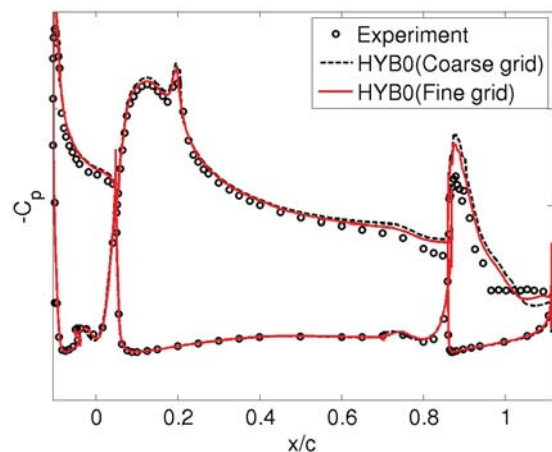


Figure 10: Surface pressure distributions computed for $\alpha = 12.2^\circ$ with the HYB0 model (with prescribed transition). The scale of C_p on the y -axis is 2.0.

The computed pressure distribution at this angle is compared with experimental measurements in Figure 10. As observed from the illustration of mean flow streamlines, the predictions obtained with both grids show only marginal difference, but are overall better than previous RANS computations for the same configuration, see e.g. Rudnik et al. (2005). With both grids, the model has disclosed a delayed boundary layer separation on the flap suction side, whilst the flap surface pressure is somewhat under-predicted (with large values of $-C_p$) prior to the separation point, particularly near the leading edge of the flap. With the fine grid, the C_p distribution in the separation bubble is slightly improved.

SUMMARY AND CONCLUSIONS

Hybrid RANS-LES modelling has been applied to turbulent flows over a three-element landing configuration exposed to a freestream with a Mach number of $M = 0.22$ at two different angles of attack. At $\alpha = 25.2^\circ$, the flow is stalled according to experimental observation, whereas the location of transition was not justified around the leading edges of the elements in the experiment. At this stall angle, the computations have been conducted using the HYB0 model and the S-A DES model with or without prescribed transition, respectively. At $\alpha = 12.2^\circ$, predictions have been produced using the HYB0 model with prescribed transition affirmed by the experiment, where two grids are invoked to explore the effect of grid resolution in the spanwise direction. The predictions are compared with experimental data for pressure distributions.

At $\alpha = 25.2^\circ$, the modelling presents rather different behavior in computations with or without prescribed transition. This is particularly true in the S-A DES modelling, where the prescribed transition triggers an unphysical laminar boundary layer separation on the slat suction side prior to the transition location. On the upper surface of the main wing after the leading edge, nonetheless, the DES computation with transition has predicted a shallow separation bubble, enabling the predicted pressure distribution in better agreement with the measured data. With prescribed transition, the HYB0 model produces relatively small surface pressures (large values of $-C_p$) over the upper surface of the slat and the main wing in comparison with the full-turbulence computation. The predicted mean flow is attached over the suction side of the whole configuration, for which the predicted pressure distribution collapses on the experimental data measured at an AoA of $\alpha = 24.4^\circ$ smaller than the stall angle ($\alpha = 25.2^\circ$). In the full-turbulence computations, both the HYB0 model and the S-A DES model have exhibited similar behavior, pronouncing boundary layer separation on the main wing suction side. The HYB0 model has produced an earlier (and slightly extended) flow separation than the S-A DES model. This flow separation leads to intensive instantaneous vortex shedding, which is extended above the flap surface, where the pressure distributions computed by both models are in very good agreement with the experimental data.

At $\alpha = 12.2^\circ$, where the transition location is justified by experimental observation, the HYB0 model performs reasonably well to resolve the instantaneous vortex motion in the trailing region of the flap. Boundary layer separation is predicted on the flap upper surface, which is however somewhat delayed, as being reflected in the comparison with the measured pressure distribution, in spite of good predictions of C_p around the slat and main wing. The grid refinement

in the spanwise direction provides marginal improvement in the prediction, most visibly, for the flow separation on the flap surface.

In view of the possible uncertainties stemmed from wind tunnel test for $\alpha = 25.2^\circ$ due to the transition location and possible 3D effects, the modelling has presented reasonable capabilities to resolve high-lift turbulent flows and to track the tendency of the flow properties moving towards stall. The HYB0 model, as well as the DES model in full-turbulence computation, may conclude a delayed stall beyond the stall incidence observed in the experiment. This will be further explored in future work, along with the specification of local transition.

REFERENCES

- Cummings, R., Morton, S., and Forsythe, J. R., 2004, "Detached-Eddy Simulation of Slat and Flap Aerodynamics for a High-Lift Wing", AIAA Paper 2004-1233, Reno, 2004.
- Davidson, L., Cokljat, D., Frhlich, J., Leschziner, M., Mellen, C., and Rodi, W. (eds), 2003, *LESFOIL: Large Eddy Simulation of Flow Around a High Lift Airfoil, Notes on Numerical Fluid Mechanics*, Vol. 83. Springer Verlag, Germany.
- Deck, S., 2005, "Zonal-Detached Eddy Simulation of the Flow Around High-Lift Configuration", *AIAA J.*, Vol. 43, pp. 2372–2384.
- Peng, S.-H., 2005, "Hybrid RANS-LES Modelling Based on Zero- and One-Equation Models for Turbulent Flow Simulation", In *Proceedings of 4th Int. Symp. Turb. and Shear Flow Phenomena*, J. Humphrey, T. Gatski, J.K.Eaton, R. Friedrich, N. Kasagi, and M. Leschziner, Eds., Vol. 3, pp. 1159–1164.
- Peng, S.-H., 2006, "Algebraic Hybrid RANS-LES Modelling Applied to Incompressible and Compressible Turbulent Flows", AIAA Paper 2006-3910. San Francisco.
- Peng, S.-H., and Eliasson, P., 2008, "Unsteady Simulation for the Flow Over a Three-Element High-Lift Configuration at Stall", AIAA Paper 2008-4143. Seattle.
- Peng, S.-H., and Leicher, S., 2008, "DES and Hybrid RANS-LES Modelling of Unsteady Pressure Oscillations and Flow Features in a Rectangular Cavity", In *Advances in Hybrid RANS-LES Modelling. Notes on Numerical Fluid Mechanics and Multidisciplinary Design.*, S.-H. Peng and W. Haase, Eds., Vol. 97, Springer, pp. 132–141.
- Rudnik, R., Eliasson, P., and Perraud, J., 2005 "Evaluation of CFD Methods for Transport Aircraft High Lift Systems", *The Aeronautical Journal*, pp. 53–64.
- Rumsey, C. L., and Gatski, T. B., 2001, "Recent Turbulence Model Advances Applied to Multielement Airfoil Computations", *AIAA Journal*, Vol. 38, pp. 904–910.
- Rumsey, C. L., and Ying, S. X., 2002, "Prediction of High Lift: Review of Present Capability", *Progress in Aerospace Sciences*, Vol. 38, pp. 145–180.
- Spalart, P. R., Jou, W.-H., Strelets, M., and Allmaras, S. R., 1997, "Comments on the Feasibility of LES for Wings and on a Hybrid RANS/LES Approach", In *Advances in DNS/LES: Proceedings of the First AFOSR International Conference on DNS/LES*, C. Liu and Z. Liu, Eds., Greyden Press, Columbus.